JOURNAL OF GUIDANCE, CONTROL, AND DYNAMICS
Vol. 24, No. 6, November–December 2001

Fast Algorithm for Prediction of Satellite Imaging and Communication Opportunities

Yan Mai* and Philip Palmer†
University of Surrey, Guildford, England GU2 7XH, United Kingdom

A new equation for nadir tracking estimation, taking into account secular perturbations from the Earth's gravitational field and the influence of drag, is presented. The advantage of this proposed approach is that it needs to be solved just twice per day with respect to a specific ground target (there are usually 14 orbital periods per day for sun synchronous orbit). The resultant approximate near nadir angle time, whose root of mean square error is around a few seconds (i.e., ~ 30-km groundtrack error), is then further refined using a newly developed controlling equation, reducing the maximum error to about 0.4 s (~ 2.8 km groundtrack) for over 20 days prediction period. This is acceptable when the imaging field of view of 10 km is considered for high resolution small satellite cameras. The prediction period of 60 days can be used for a typical small satellite camera whose field of view is about 100 km. This method can also be expanded to solve the rise-and-set time problem. Because of the low complexity of the proposed method, it is very suitable for implementation on the onboard processor whose computational resources are generally limited. The new computational process is described and simulation results are presented.

Nomenclature

a	=	satellite's orbital semimajor axis
h	=	elevation angle
i	=	inclination
N	=	integer representing the number of satellite passages
n	=	mean motion
r	=	radial distance of the satellite from the center of the Earth
T	=	orbital period
t_0	=	time when the satellite first crosses over a given latitude line on the ascending pass
γ	=	angle of camera field of view
$\Delta\upsilon_{\max}$	=	maximum longitudinal offset angle for target to be in field of view of camera
θ_υ	=	longitudinal angle margin for ground target to be visible to satellite
λ	=	argument of latitude measured on orbital plane
υ_S	=	geodetic longitude of satellite footprint
υ_T	=	geodetic longitude of ground target
φ_T	=	geocentric latitude of ground target
ϕ_T	=	geodetic latitude of ground target
Ω	=	right ascension of ascending node
ω	=	argument of perigee
$\omega_\oplus$	=	Earth rotation rate

I. Introduction

FUTURE generations of Earth observation satellites must be considerably more operable and autonomous to enable continuing military and civil applications such as resources investigation, fast-changing phenomenon monitoring, and geographic information generation. The need for greater operability and autonomy stems from shrinking governmental support for imaging space missions and commercial interest in deploying low-cost small satellites for Earth observation. Greatly decreased operations costs will not only enable more such missions, but will also enable systems to be scalable to meet commercial goals. These include ESAT (URL: http://www.dbsindustries.com/investor.html#esat), which consists of a 6 enhanced microsatellite constellation targeted at the gas and electric utility for Global Energy Metering Service (GEMS); Global Altimeter Network Designed to Evaluate Risk,[1] which operates a constellation of 16 small satellites that will orbit the Earth in rapid succession, observing sea surface winds and waves so that ships at sea can be constantly updated on the sea conditions around them; and a proposed 7-microsatellite constellation[2,3] to deliver global frequent disaster monitoring. Accordingly, the number of users of Earth images will increase rapidly. Among all sorts of spacecrafts carrying imaging instruments, low-cost small satellites will become a main source because of their cost effectiveness and fast reaction.

With the increasing capability of modern micro- and minisatellites to undertake autonomous imaging of targets on the surface of the Earth by employing sophisticated onboard computers and data processing techniques, one requirement is to be able to determine the time of closest approach to nadir of a satellite in low Earth orbit for a specific ground location. Because the satellite may not fly directly over the desired target area for some period (days or weeks), it is first necessary to determine whether a given target will be within the narrow field of view of the satellite cameras to capture an image within a shorter time span. In the conventional approach, it has been customary to solve this problem by letting the satellite run through its ephemeris and then checking at each instant to see where the subsatellite nadir point falls. An orbital simulation is advanced in time by some small time increment Δt, and a possibility check is performed at each step. This method is called trajectory checking. However, this method requires Keplerian equations to be solved hundreds of times per orbital period, and is, therefore, not suitable for onboard processing because of the computational load.

A closely related problem is the rise-and-set time problem of when a satellite is visible from a given point on the Earth. An important application of this is to find when the satellite is visible over a ground station for data transmission. The simplest way to solve this problem is by using a numerical method such as described in the preceding paragraph. Escobal[4] proposed a faster method to solve this problem by developing a closed-form solution for the visibility periods. He introduced a single transcendental equation as a function of the eccentric anomaly of the satellite orbit, which he called the controlling equation. Numerical methods[5] were then used to find the rise-and-set times. The advantage of this equation is that it is solved only once per orbital period, in contrast with the hundreds of times the Keplerian equation must be solved with the standard step-by-step technique of hill climbing. The controlling equation, however, is only valid for two-body motion, and our main aim is to solve

Received 13 June 2000; revision received 29 August 2000; accepted for publication 4 December 2000.

*Ph.D. Student, Surrey Space Centre.
†Senior Lecturer, Surrey Space Centre.

the satellite nadir tracking problem, which means in application this equation needs further development.

Besides the controlling equation method, Lawton[6] has developed another method to solve for satellite–satellite and satellite–ground station visibility periods for vehicles in circular or near circular orbits by approximating the visibility function $\psi(t)$ by a Fourier series. More recently, Alfano and Negron[7] (see also Ref. 8) further developed the $\psi(t)$ function to suit all orbital types. However, these methods are only valid for solving satellite rise-and-set time problems and are not suitable for satellite nadir tracking and still have their own limitations.

In this paper, a new method is presented that can be used not only for two-body motion, but also accommodates secular perturbations, short and long periodic perturbations, and the influence of drag in a straightforward manner, providing a simple equation for nadir tracking and solving the satellite visibility problem. The proposed formulation only needs to be solved twice per day, which makes it very suitable for implementation onboard a small satellite. In Sec. II, we describe the first phase of the new method, which is called coarse search. It works in two-body, secular perturbations arising from the Earth's oblateness and atmospheric drag perturbations. In Sec. III, we introduce the second phase of the method, which is called refinement. Refinement improves the accuracy of the new method. Simulation results are presented in Sec. IV, as well as the comparison of CPU processing time between the conventional method and this new method. Finally, in Sec. V, we set out our conclusions.

II. Coarse Search for Satellite Passes

A. Fundamental Algorithm: Two-Body Analysis

We can easily estimate the satellite closest approach time by checking the satellite ascending and descending passage once, respectively, per day. Set the orbital period of the satellite to be $T(=2\pi/n)$ (where n is the mean motion) and t_0 the time when the satellite first crosses over a given latitude line on the ascending pass (Fig. 1). We call the circle of constant latitude that runs through the target location the target latitude line (TLL). The key point of our approach is to use the fact that, for two-body motion, a satellite will revisit exactly the same point in an inertial coordinate system after each orbital period T (Fig. 1). This means that the satellite will make another ascending pass over the TLL at time $(t_0 + T)$. To simplify the discussion, we shall ignore the descending passages over the TLL and include them again only at the end. Note that in this method satellite position is expressed by the redundant epicycle coordinates r, λ, I, and Ω (Ref. 9), where r is the radial distance of the satellite from the center of the Earth, λ is the argument of latitude measured on the orbital plane, i is the inclination, and Ω is the right ascension of the ascending node.

If the location of a target on the Earth is (υ_T, ϕ_T), where υ_T and ϕ_T are the geodetic longitude and latitude, respectively, then the satellite will pass over the TLL every $t_0 + NT$ (or $t_0 + N2\pi/n$), where N is an integer representing the number of satellite passages.

At time t_0, the satellite is over the TLL and the initial longitudinal difference between the satellite footprint υ_S and target υ_T is $\Delta\upsilon = \upsilon_S - \upsilon_T$. After each orbital period the satellite revisits the TLL and the Earth rotates under it, bringing the target closer to the satellite's longitudinal position. The satellite will see the target approaching by an amount $\omega_\oplus T$ or $\omega_\oplus 2\pi/n$, where $\omega_\oplus$ is the Earth's rotation rate. The target closest satellite passage (TCSP) occurs when the longitudinal difference $d\upsilon$ is smaller than $\omega_\oplus 2\pi/n$. Therefore, we obtain the following fundamental equation:

$$\Delta\upsilon = N\omega_\oplus 2\pi/n + d\upsilon \tag{1}$$

where $d\upsilon$ is the longitudinal difference between the subsatellite point and the target at TCSP.

Hence,

$$N = [(\Delta\upsilon/2\pi)(n/\omega_\oplus)] \tag{2}$$

where the square brackets implie the integer part.

In other words, the closest approach to the target will occur when $0 \le d\upsilon < \omega_\oplus 2\pi/n$. Therefore, as long as we know the initial passage time t_0 of the TLL and the satellite's orbital period T, we can derive the possible closest approach time over long intervals of time. We name the procedure of TCSP estimation as coarse search because the satellite maximum elevation time over the target does not necessarily occur at TLL crossing.

Even in this TCSP case, however, the satellite maximum elevation angle of this pass may not be suitable for imaging because the onboard camera field of view (FOV) is very small. Therefore, we need to find the maximum longitudinal offset angle $\Delta\upsilon_{\max}$ for the target to be in the FOV of the camera and to check whether $d\upsilon \le \Delta\upsilon_{\max}$. The calculation of $\Delta\upsilon_{\max}$ will be described in Sec. II.A.2.

To determine the rise-and-set times of the satellite over a given ground station, some modification to the description given has to be made. Instead of $\Delta\upsilon_{\max}$, we need to set another angle margin θ_υ within which the ground target is visible to the satellite (Fig. 2). Vallado and McClain[8] define this as the ground-range angle. The calculation of θ_υ will be described in Sec. II.A.2. Figure 3 shows the

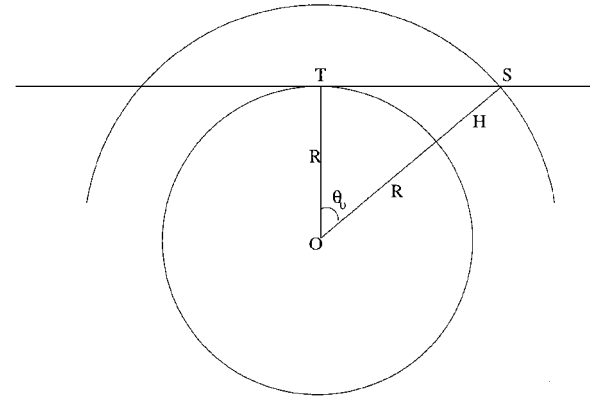

Fig. 2 Within longitude angle θ_υ satellite S is visible to ground target T.

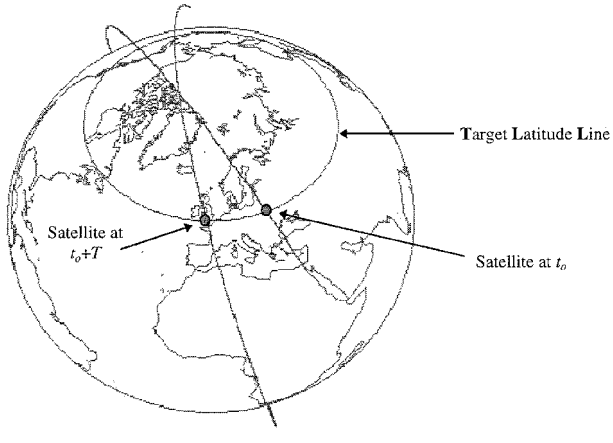

Fig. 1 Satellite orbiting around Earth showing crossings of TLL.

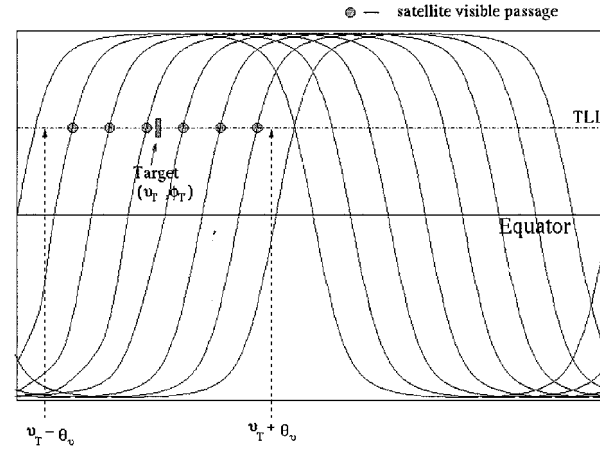

Fig. 3 Visibility of satellite passes.

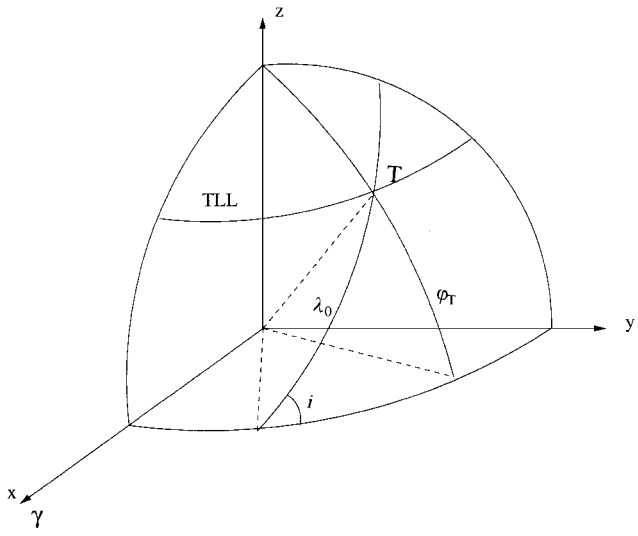

Fig. 4 Geometry of λ_0 in Earth-centered inertial coordinate.

basic idea of our new method for satellite rise-and-set times. When the satellite is visible, its longitude υ_S must satisfy the following condition:

$$\upsilon_T - \theta_\upsilon \le \upsilon_S \le \upsilon_T + \theta_\upsilon \tag{3}$$

To test whether the passes are visible, we start from $\upsilon_S \simeq \upsilon_T - \theta_\upsilon$. If this is a visible pass, we add it to our coarse search list. When $\upsilon_S < \upsilon_T - \theta_\upsilon$, we add 2π to υ_S. When $\upsilon_S > \upsilon_T + \theta_\upsilon$, we can compute the difference in longitude $\Delta\upsilon_\upsilon = \upsilon_S - (\upsilon_T + \theta_\upsilon)$ that will bring it to within the visibility of the ground station. Therefore, we get the following formula for satellite visible estimation:

$$N = [(\Delta\upsilon_\upsilon/2\pi)(n/\omega_\oplus)] + 1 \tag{4}$$

1. Finding Initialization Argument of Latitude λ_0

In the preceding section, we pointed out that we need to know the initial passage time t_0 of the TLL. In our approach, we only need to calculate the corresponding initial υ_{S0}. Therefore, we need λ_0 (the initial argument of latitude) for TLL. This is found from the spherical triangle shown in Fig. 4, where T is the ground target and φ_T is the geocentric latitude of the ground target:

$$\sin\lambda_0 = \sin\varphi_T / \sin i \tag{5}$$

2. Longitudinal Offset Angle Margin

a. Angle margin for satellite maximum elevation angle estimation. For nadir tracking, sometimes the satellite maximum elevation angle to a specific target may not be high enough for the payload to image the ground target. Therefore, we need to find the longitudinal offset angle, which determines whether a given passage is a suitable closest approach passage. The range of an image is dependent on the physical dimension of the charge-coupled device (CCD) array and the focal length of the lens. For the narrow angle camera of PoSAT-1,[10] which has an interlaced CCD matrix of dimension 576×560 (about 8.4×6.5 mm) and focal length of 50 mm, the ground cover is 150×100 km from an orbital altitude of 800 km, which corresponds to the camera's half FOV of 3.6 deg. For nadir tracking, we need to find the longitudinal offset angle margin $\Delta\upsilon_{\max}$ to check whether the previous approach estimation would be acceptable, which means we need to check whether $d\upsilon \le \Delta\upsilon_{\max}$.

We assume the shape of the Earth is spherical. Let the camera FOV angle be γ. Then the upper limit of the spherical offset angle $\theta(r)$ is given by (Fig. 5)

$$\theta(r) = \sin^{-1}[(r/a_e)\sin(\gamma/2)] - \gamma/2 \tag{6}$$

where r is the geocentric range of the satellite and a_e is the Earth's equatorial radius. Vallada and McClain[8] describe in detail the geometry of surveillance and reconnaissance operations.

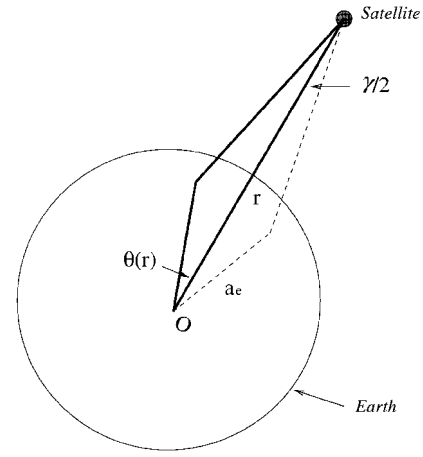

Fig. 5 Location of target and satellite at closest approach; *O* is center of Earth, where offset angle θ is defined; γ is FOV of camera.

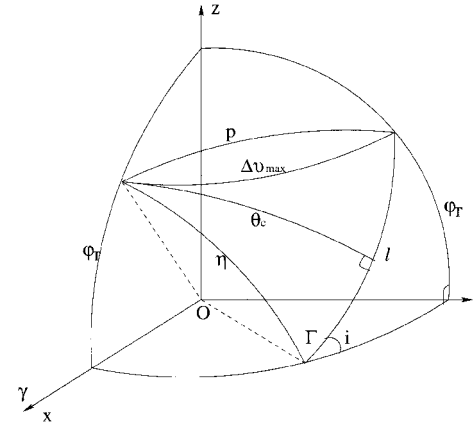

Fig. 6 Computation of maximum longitudinal offset angle margin $\Delta\upsilon_{\max}$, given ground track of satellite(l) and spherical offset angle θ_c.

For typical Earth observation orbits, which are near circular and polar, the angle $\theta(r)$ in Eq. (6) can be approximated by the constant angle

$$\theta_c = \sin^{-1}[(a/a_e)\sin(\gamma/2)] - \gamma/2 \tag{7}$$

where a is the satellite's orbital semimajor axis. From the angle θ_c, we can compute the longitudinal offset angle margin $\Delta\upsilon_{\max}$. Figure 6 shows how $\Delta\upsilon_{\max}$ is related to the satellite inclination angle i, the upper limit of the spherical offset angle θ_c, and ground target latitude φ_T. The arc l represents the satellite's ground track. To find $\Delta\upsilon_{\max}$, we start by finding p. Then the longitudinal offset angle $\Delta\upsilon_{\max}$ can be solved by following the equation for a small circle (Werts,[11] page 727, Eq. A-3):

$$\cos\Delta\upsilon_{\max} = \frac{\cos p - \sin^2\varphi_T}{\cos^2\varphi_T} \tag{8}$$

To find p we use the law of cosines for sides (Werts,[11] page 732, Eq. A-26):

$$\cos p = \cos l\cos\eta + \sin l\sin\eta\cos\Gamma \tag{9}$$

where the three angles of l, η, and Γ are given in terms of φ_T, θ_c, and i using the law of sines (Werts,[11] page 732, Eq. A-25):

$$\tan\Gamma = \frac{\sin\theta_c\sin i}{\sin\varphi_T - \cos i\sin\theta_c} \tag{10}$$

$$\sin\eta = \frac{\sin\theta_c}{\sin\Gamma} \tag{11}$$

$$\sin l = \frac{\sin\varphi_T}{\sin i} \tag{12}$$

This completes the approach estimation procedure.

b. Angle margin for rise-and-set times. The rise time of a satellite should occur when the satellite, at a given orbital height, crosses the horizon plane. In this case, we set up another angle margin θ_υ as shown in Fig. 2 and simplified the calculation for it.

If the orbital radius of the satellite S is $a(=R+H$, where R is the radius of the Earth and H is the satellite orbital height) then (see Ref. 8):

$$\cos\theta_\upsilon = R/a \tag{13}$$

We, therefore, wish to estimate the times when the satellite reaches the target longitude within $\pm\theta_\upsilon$. However, because this a simplified calculation for satellite longitudinal angle margin, we reduce R by a fixed fraction to avoid missing some low passes.

B. Adding Secular Perturbations

A satellite under the influence of an inverse square gravitational law has truly constant orbital elements. In reality, however, there is a gradual change in the orbital elements due to the Earth's oblateness. The principal effect of this is to introduce a short-period oscillation of the orbital elements, which we can ignore in most cases. The argument of perigee ω and longitude of the ascending node Ω, however, experience a secular drift that significantly changes the long-term prediction of maximum elevation angle. We can adopt the method we have outlined in Sec. II.A to take proper account of all of these secular variations. In the following description we will introduce the formulas for the satellite maximum elevation angle prediction. The procedure for satellite rise-and-set times is similar to this.

First, we can easily add secular perturbations to the coarse search procedure for the effect on the argument of latitude λ that changes the nodal period if the satellite comes back to the same TLL:

$$\lambda = \alpha(1+\kappa) \tag{14}$$

where κ is the coefficient of secular drifts in the epicycle equations[9] and epicycle phase $\alpha = nt$. Thus, there is a change in α for each TLL crossing of $\Delta\alpha = 2\pi/(1+\kappa)$.

The second effect is the precession of the orbital plane $\dot{\Omega}$. This moves the target away from the orbital plane, $\dot{\Omega} > 0$. We can incorporate this effect into the rotation rate of the Earth:

$$\omega_{\text{eff}} = \omega_\oplus - \dot{\Omega} \tag{15}$$

In the epicycle description of the orbit,[9] the variation in Ω is expressed as

$$\Omega = \Omega_0 + \theta\alpha \tag{16}$$

where θ is the secular coefficient of plane precession.[9] Hence, $\dot{\Omega} = \theta n$.

We can incorporate these results into Eqs. (1) and (2) for the coarse search to get

$$\Delta\upsilon = (\omega_\oplus - \theta n)N(\Delta\alpha/n) \tag{17}$$

Therefore,

$$N = \left[\frac{\Delta\upsilon}{2\pi}\frac{n(1+\kappa)}{(\omega_\oplus - \theta n)}\right] \tag{18}$$

C. Accounting for Drag

Gravity is not the only force acting on the satellite. Another important effect comes from the Earth's atmosphere, which still has a significant effect on orbits up to altitudes as high as 1000 km. Because most of our Earth observation satellites orbit at altitudes lower than this, we need to consider the effects of atmospheric drag. Drag is very difficult to model because of the many factors affecting the Earth's upper atmosphere and the satellite's attitude, which affects the cross-sectional area. In this paper, we only consider the effect of drag on the satellite's argument of lattitude for the coarse search and include the effect on r in the refinement. To test our result, the SGP4 model[12] has been used for drag modeling.

The effect of drag on the argument of latitude can be incorporated into the epicycle equations as

$$\lambda = \alpha(1+\kappa) + 1.5B\alpha^2 \tag{19}$$

where B is the drag coefficient.

We start by finding the change in the epicycle phase α over one nodal period. By setting λ to be 2π, we find the solution for $\alpha(=\Delta\alpha)$ from Eq. (19):

$$\Delta\alpha = [4\pi/(1+\kappa)]\cdot\left[1\Big/\left(1+\sqrt{1+12\pi B}\right)\right] \tag{20}$$

Using this in Eq. (17), we obtain

$$N = \{(\Delta\upsilon/\Delta\alpha)[n/(\omega_\oplus - \theta n)]\} \tag{21}$$

This completes our discussion of the coarse search, where we have included the secular perturbations and atmospheric drag.

III. Refining the Estimates of Maximum Elevation and Rise-and-Set Times

Having estimated the approach time to the target at TLL, we now need a procedure that will refine this estimate to an application set tolerance. For this we extend Escobal's[4] approach to determine the maximum elevation angle by introducing a new controlling equation based on the epicycle equations.

In Fig. 7, we show the geometry of a satellite pass. The target ground station T is located on the surface of an oblate Earth, and the vector z_T is the local normal to the ground target surface. The position of the satellite is S. We have the position of both the target and the satellite in Earth-centered, Earth-fixed (ECEF) coordinates[13] expressed in r, I, Ω, λ, and α from the epicycle equations, from which we compute the slant vector $\boldsymbol{P}$:

$$\boldsymbol{P} = \boldsymbol{X}_S - \boldsymbol{X}_T \tag{22}$$

This gives the position of the satellite as seen from the target. The elevation angle is the angle measured from the horizon up to the satellite. If this angle is h, then

$$\boldsymbol{P}\cdot\boldsymbol{Z}_T = P\sin h \tag{23}$$

Therefore, we name a new controlling equation:

$$F(\alpha) = \sin h = (\boldsymbol{P}\cdot\boldsymbol{Z}_T)/P \tag{24}$$

F is a function of α only through $\boldsymbol{X}_s$, and $\boldsymbol{Z}_T$ and $\boldsymbol{X}_T$ are constant vectors in the ECEF coordinate system. $\boldsymbol{X}_s$ varies with α both because the satellite moves along its orbits and through the Earth's rotation in the transformation from Earth-centered inertial[13] to ECEF coordinates. It is obvious that the maximal and zero points of the elevation angle h represent the maximal and zero of function $F(\alpha)$, respectively. Therefore, to find the maximum elevation angle, we just need to find $\alpha_{\max}$ such that $\mathrm{d}F/\mathrm{d}\alpha(\alpha_{\max}) = 0$, in which case we

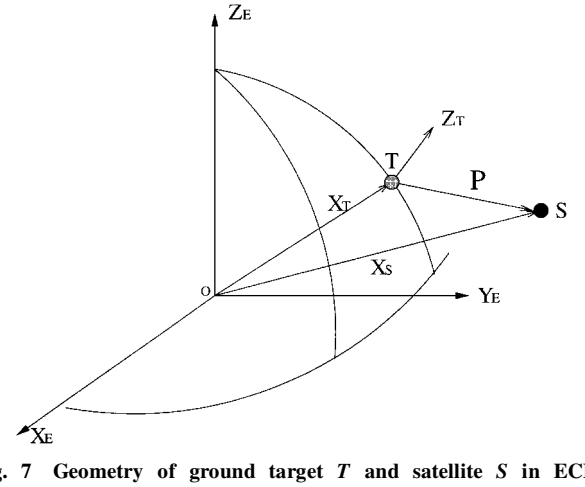

Fig. 7 Geometry of ground target T and satellite S in ECEF coordinates.

take the derivative of $F(\alpha)$, and the solution should represent the satellite maximum elevation time.

The computation of satellite location $\boldsymbol{X}_S$ is carried out as follows.

The epicycle equations which express (r, I, Ω, λ) as functions of time can be written as

$$r = a(1+\rho) - A\cos(\alpha - \alpha_p) + a\chi \sin\beta + a\Delta_r \cos 2\beta - 2B\beta \tag{25}$$

$$I = I_0 + \Delta_I(1 - \cos 2\alpha) \tag{26}$$

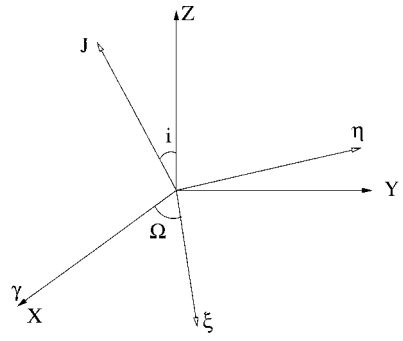

Fig. 8 Earth-centered inertial coordinates (X, Y, Z) and orbital plane coordinates (ξ, η, J).

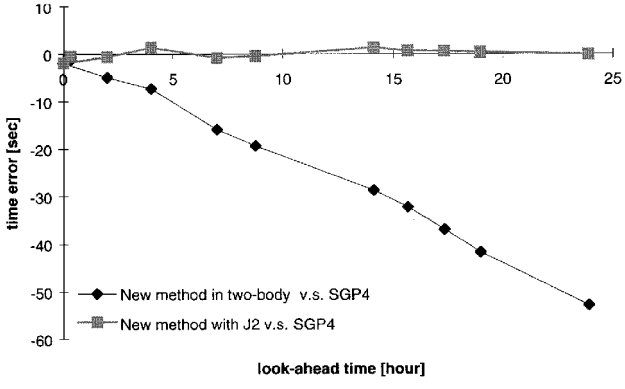

Fig. 9 Diamonds show timing error of two-body prediction when compared with SGP4 model; squares show error when J_2 is incorporated.

$$\Omega = \Omega_0 + \theta\alpha + \Delta_\Omega \sin 2\alpha \tag{27}$$

$$\lambda = \beta + (2A/a)[\sin(\alpha - \alpha_p) + \sin\alpha_p] - 2\chi(1 - \cos\beta) + \Delta_\lambda \sin 2\beta + \tfrac{3}{2}B\beta^2 \tag{28}$$

where we have included the effects of atmospheric drag,[14] and

$$\beta = (1 + \kappa)\alpha \tag{29}$$

where ρ, κ, and θ are the coefficients for secular perturbation; χ represents long periodic perturbation coefficients; and Δ represents the short periodic terms.

We define the satellite position (ξ, η) (Fig. 8) on the orbital plane using Cartesian coordinates with the ξ axis along the ascending node of the orbit. Hence,

$$\xi = r\cos\lambda, \qquad \eta = r\sin\lambda$$

$\boldsymbol{X}_S$ can be expressed in ECEF coordinates as $\boldsymbol{X}_S = (X_E, Y_E, Z_E)$, where

$$\begin{aligned} X_E &= \xi\cos(\nu - \Omega) + \eta\cos I\sin(\nu - \Omega) \\ Y_E &= -\xi\sin(\nu - \Omega) + \eta\cos I\cos(\nu - \Omega) \\ Z_E &= \eta\sin I \end{aligned} \tag{30}$$

and ν is the local ephemeris time (the angle between the first point of Aries γ and the X_E axis in the ECEF frame). These equations together describe the dependence of F on α.

IV. Test and Result

Results for two-body and secular perturbation expansion are as follows.

For many practical problems, the approximation of two-body motion is sufficient, especially if two closely neighboring points on a trajectory are under investigation. However, for the long-term satellite passes prediction, we cannot ignore the cumulative effect of the gradual variation of elements from their two-body values to achieve the required accuracy for satellite imaging and communication. In Fig. 9, we show the prediction of our method compared with the SGP4 model.[12] The diamonds clearly indicate that after only a few hours the timing error of our prediction based on two-body theory is already up to 8 s, and within one day the timing error is around 1 min. Images from PoSAT-1 cover an area 150 × 100 km on the

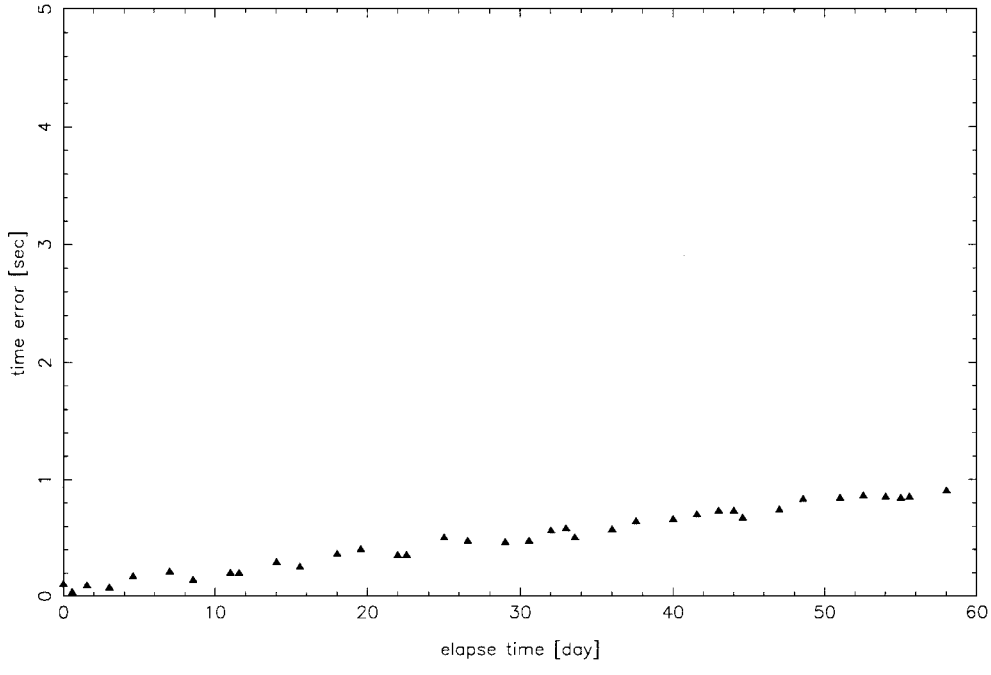

Fig. 10 Timing errors when short and long variations are included, when compared with SGP4.

ground which means that the prediction timing errors should be at least within 7 s (1 s corresponds to approximately 7 km ground-track) to keep the target within the image. The two-body prediction is, therefore, only adequate for image capture within $2 \sim 3$ h.

To reduce the timing errors, we have included the secular effects into our coarse search. Unlike Escobal's[4] original controlling equation, our function $F(\alpha)$ not only includes secular drift but also has short- and long-periodic perturbations taken into account. We present in Table 1 a comparison of the epicycle prediction with an accurate propagator[15] to look at the timing errors from the prediction when atmospheric drag is ignored. Table 1 shows that the timing errors are as small as 0.15 s for a look-ahead time of almost 300 days.

In Fig. 10 we show a comparison of our prediction with SGP4. With an exhaustive search approach we see that the timing difference between our method and SGP4 is less than 1 s for two months look-ahead time. As Mai and Palmer[16] pointed out, when atmospheric drag can be ignored, the difference between our prediction and SGP4 arises because the accuracy of SGP4 is only 10^{-6}, and there is a small drift of λ between the epicycle equations and SGP4 that builds up to a significant error. This demonstrates that over a look-ahead time of a few days, when drag effects can be ignored, we have achieved the prediction timing accuracy required by the high-resolution camera on UoSat-12 (Ref. 17).

We next consider the drag compensation that we introduced in Sec. II. In Fig. 11, we show the timing errors compared with SGP4, now with drag included in the model. Both predictions are based on the same set of initial conditions taken for the same North American Aerospace Defence Command (NORAD) file (URL:http://www.celestrak.com), and the predictions extend over 100 days. With a look-ahead time of 100 days, the timing error has now been reduced to about 2 s. Without drag compensation, for the

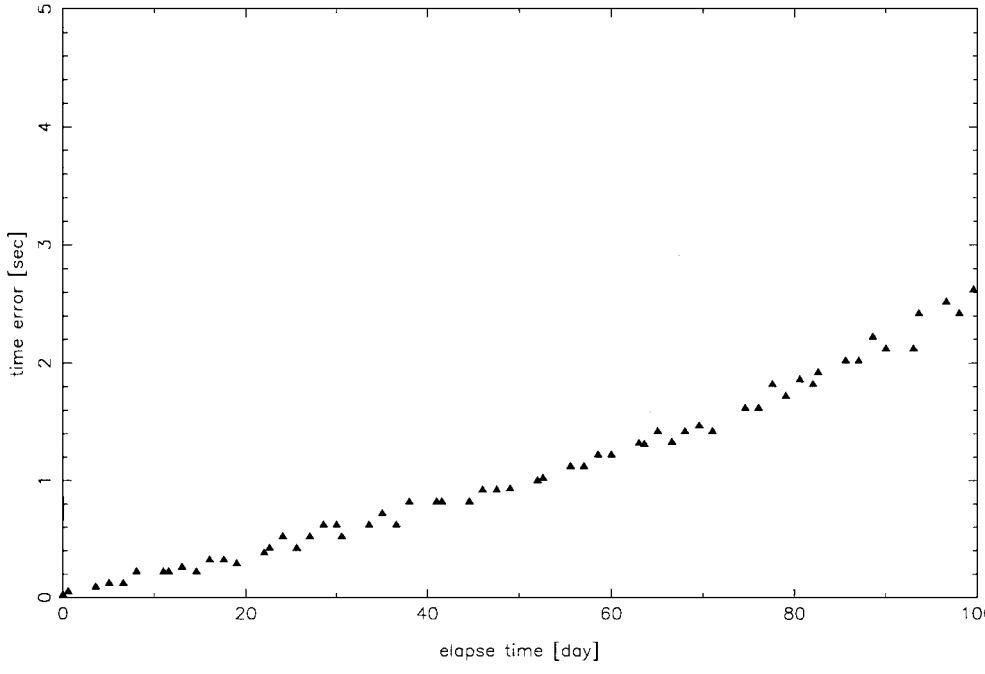

Fig. 11 Timing errors when atmospheric drag is included, when compared with SGP4.

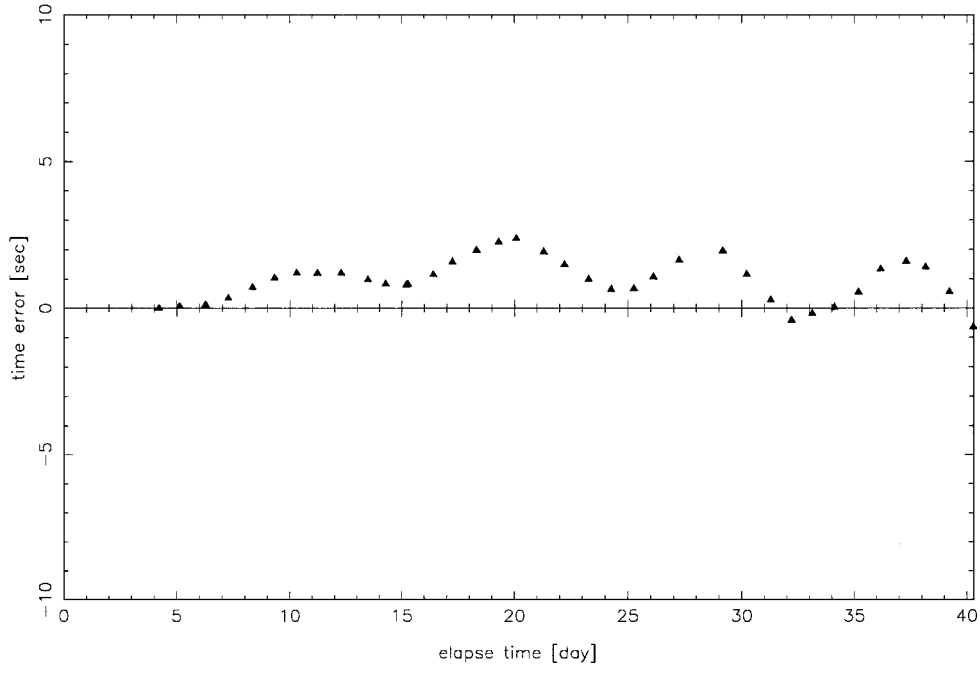

Fig. 12 Prediction errors of single pass using our method, for look-ahead times of up to 40 days using NORAD data at different epochs.

Table 1 Timing errors as a function of look-ahead time, comparing the predictions with an accurate orbit propagator

Look-ahead time, day	Timing error, s
0.96	$8.7e-3$
4.53	$2.2e-2$
9.26	$3.8e-2$
——	——
298.99	$1.5e-1$

Table 2 Processing time on a Pentium II, averaged over 10,000 experiments[a]

Proposed method	Estimation, s	Refining, s
Two-body	1.71	2.86
J_2	1.86	3.71

[a]Current program, SGP4 = 786 s.

same accuracy level, the look-ahead time is only one week. Thus, for PoSAT-1, with a typical small satellite remote sensing camera, we can predict imaging opportunities for up to 100 days ahead. For UoSat-12, which has a high-resolution camera onboard, we can predict imaging opportunities for up to 1 month with sufficient accuracy.

To remove the drift errors in SGP4, we performed one last experiment where we compared the predictions of our algorithm with itself, using two different NORAD files. The separation in time between the two NORAD files was anything up to 40 days, and the timing errors for the same pass are shown in Fig. 12. One of these predictions was based on a NORAD data set from just before the pass. The dates used for this experiment were from May to July of 1997. The variability in prediction time is due to the variability of atmospheric drag.

The algorithm is several orders of magnitude faster to run than the exhaustive search using SGP4 that we have employed. In Table 2 we present some timings for the estimation on a Pentium II. These timings are sufficiently short for this algorithm to be used on hand-held receivers and are sufficiently accurate to control imaging devices on satellites.

V. Conclusions

We have introduced a new method to predict the passes of a satellite's closest approach to a specific target on the ground. This is useful for satellite nadir tracking and solving the satellite visibility problem. We have first described a coarse search phase of this method, including two-body motion, secular perturbation, and atmospheric drag. We have then described the second phase, refinement, which uses a further developed controlling equation $F(\alpha) = 0$ based on the epicycle equations. We have shown that, ignoring drag effects, we can achieve timing accuracies of 1 s for look-ahead times of 60 days. When drag compensation is included, we provide sufficiently accurate timing estimates for over 100 days ahead. For most imaging and communication applications using small satellites, this is sufficient. For high-resolution imaging, look-ahead time is reduced to about 1 month.

Although we have shown that, particularly as we approach solar maximum, the variability of atmospheric drag degrades performance, it is still adequate to predict imaging times to within 1–2 s over a timescale of a month. Estimates can be automatically updated during this interval to monitor the stability of the image capture time and, hence, remove the effects of the uncertainty in the drag parameters.

We have shown elsewhere[16] how to translate NORAD elements, which are freely available for all traded satellites over the Internet, to epicycle elements. Hence, this method can be used by any system that has access to these NORAD files.

Acknowledgments

The authors are grateful for the financial support of the Surrey Space Centre (SSC) and Surrey Satellite Technology Limited. The authors wish to acknowledge the support given by Martin Sweeting of SSC.

References

[1]Da Silva Curiel, R. A., Sun, W., Sweeting, M., Jolly, G., and Stephens, P., "The 'GANDA' Mission," International Academy of Astronautics, Paper IAA-00-IAA.11.4.05, Oct. 2000.

[2]Chu, V., Da Silva Curiel, R. A., Sun, W., and Sweeting, M., "Disaster Monitering Constellation," International Academy of Astronautics, Paper IAA-00-IAA.11.4.03, Oct. 2000.

[3]Sweeting, M., and Chen, F. Y., "Network of Low Cost Small Satellites for Monitoring and Mitigation of Natural Disasters," International Astronautical Federation, Paper IAF-96-B.3.P215, Oct. 1996.

[4]Escobal, P. R., *Methods of Orbit Determination*, Wiley, New York, 1976, pp. 162–174.

[5]Burden, R. L., and Faires, J. D., *Numerical Analysis*, 6th ed., Cole Publishing, New York, 1997, pp. 65–78.

[6]Lawton, J. A., "Numerical Method for Rapidly Determining Satellite–Satellite and Satellite–Ground Station In-View Periods," *Journal of Guidance, Control, and Dynamics*, Vol. 10, No. 1, 1987, pp. 32–36.

[7]Alfano, S., Negron, D., Jr., "Rapid Determination of Satellite Visibility Periods," *Journal of Astronautical Sciences*, Vol. 40, No. 2, 1992, pp. 281–296.

[8]Vallado, D. A., and McClain, W. D., *Fundamentals of Astrodynamics and Applications*, McGraw–Hill, New York, 1997, pp. 741–815.

[9]Hashida, Y., and Palmer, P., "Epicyclic Motion of Satellites About an Oblate Planet," *Journal of Guidance, Control, and Dynamics* (to be published).

[10]Fouquet, M., Sweeting, M. N., "Earth Observation Using Low Cost Micro/Minisatellites," *Acta Astronautica*, Vol. 39, No. 9/12, 1996, pp. 823–826.

[11]Wertz, J. R., *Spacecraft Attitude Determination and Control*, D. Reidel, Dordrecht, The Netherlands, 1978, pp. 727, 732.

[12]Hoots, F. R., and Roehrich, R. L., "Models for Propagation of NORAD Element Sets," Aerospace Defense Center, Spacetrack Rept. 3, Peterson, AFB, CO, 1980, pp. 10–20.

[13]Chobotv, V. A., *Orbital Mechanics*, 2nd ed., AIAA, Reston, VA, 1996, pp. 11–16.

[14]Hashida, Y., and Palmer, P., "Epicycle Motion of Satellites Under the Atmospheric Drag Perturbation," (submitted for publication).

[15]Palmer, P. L., Aarseth, S. J., Mikkola, S., and Hashida, Y., "High Precision Integration Methods for Orbit Propagation," *Journal of Astronautical Sciences*, Vol. 46, No. 4, 1998, pp. 329–342.

[16]Mai, Y., and Palmer, P. L., "Conversion of North American Aerospace Defence Command Elements to Epicycle Elements," *Journal of Guidance, Control, and Dynamics*, Vol. 24, No. 2, 2001, pp. 406–408.

[17]Fouquet, M., and Sweeting, M., "UoSAT-12 Minisatellite for High Performance Earth Observation at Low Cost," *Acta Astronautica*, Vol. 41, No. 3, 1997, p. 173–182.